Technical Report
865

A Space-Based Optical Communication System Utilizing Fiber Optics

E.A. Swanson
R.S. Bondurant

9 November 1989

Lincoln Laboratory
MASSACHUSETTS INSTITUTE OF TECHNOLOGY
LEXINGTON, MASSACHUSETTS

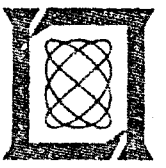

Prepared for the Department of the Air Force
under Contract F19628-90-C-0002.

This report is based on studies performed at Lincoln Laboratory, a center for research operated by Massachusetts Institute of Technology. The work was sponsored by the Department of the Air Force under Contract F19628-90-C-0002.

The ESD Public Affairs Office has reviewed this report, and it is releasable to the National Technical Information Service, where it will be available to the general public, including foreign nationals.

This technical report has been reviewed and is approved for publication.

FOR THE COMMANDER

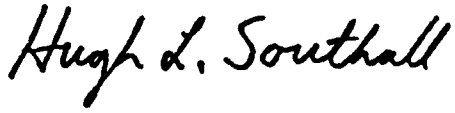

Hugh L. Southall, Lt. Col., USAF
Chief, ESD Lincoln Laboratory Project Office

MASSACHUSETTS INSTITUTE OF TECHNOLOGY
LINCOLN LABORATORY

A SPACE-BASED OPTICAL COMMUNICATION SYSTEM UTILIZING FIBER OPTICS

E.A. SWANSON
R.S. BONDURANT
Group 67

TECHNICAL REPORT 865

9 NOVEMBER 1989

LEXINGTON MASSACHUSETTS

ABSTRACT

The use of fiber optics to simplify the design of free-space laser communication systems is explored. The potential advantages of fiber optics within free-space optical communication systems are not widely recognized. The current generation of spaceborne optical communication systems relies on the use of bulk optics rigidly mounted to an optical bench to get light from the optical sources to the exit aperture or from the entrance aperture to the optical receiver. These designs are all very sensitive to thermal and mechanical perturbations as well as to the detailed dynamic characteristics of the host spacecraft. Optical fibers can provide the means to remotely locate the transmitter lasers, local oscillator (LO) lasers (in the case of a coherent system), and the receiver from the front-end optics. This allows flexibility in the mechanical design which can reduce the size, weight, and stability requirements of the overall system.

This paper presents an overview of a fiber-based free-space lasercom system and contrasts this proposed technology to the present technology. Detailed design considerations concerning the issues of pointing, tracking, and receiver communication performance are presented. Other key areas such as efficient source-to-fiber coupling, isolation, transmitter power limitations, and acquisition are highlighted. Preliminary experimental results of our breadboard fiber-based coherent optical communication system are also presented.

ACKNOWLEDGMENTS

We would like to acknowledge the valuable contributions from James Roberge who helped designed and build many of the electronic circuits used in the experiments and helped develop many of the ideas used in the overall system design, Linden Mercer who helped in analyzing the effects of feedback from optical fibers, and Ronald Sprague who built most of the mechanical components.

TABLE OF CONTENTS

	Abstract	iii
	Acknowledgments	v
	List of Illustrations	ix
	List of Tables	xi
1.	INTRODUCTION	1
2.	SYSTEM OVERVIEW	3
3.	NUTATING FIBER RECEIVER	5
	3.1. Overview	5
	3.2. Communication Performance	7
	3.3. Noise Equivalent Spectral Density	10
	3.4. Resonant Fiber Coupler	15
	3.5. Tracking Loop Rejection	17
	3.6. Acquisition	17
4.	TRANSMITTER	21
	4.1. Overview	21
	4.2. Transmitter Fiber Coupler	22
	4.3. Transmitter Module	24
	4.4. Strawman Transmitter Power Loss Budget	26
5.	CONCLUSION AND DISCUSSION	29
	APPENDIX	31
	REFERENCES	35

LIST OF ILLUSTRATIONS

Figure No.		Page
2-1	Optical schematic.	3
3-1	Nutating fiber receiver.	5
3-2	Fiber coupling profile.	6
3-3	Tracking system diagram.	7
3-4	Communication channel loss vs relative signal beam diameter and nutation depth.	8
3-5	Tracking channel loss vs relative signal beam diameter and nutation depth (SNR>>1).	11
3-6	Tracking channel loss vs relative signal beam diameter and nutation depth (SNR<<1).	12
3-7	Communication and tracking loss vs nutation depth.	13
3-8	NEA vs signal power.	14
3-9	Breadboard resonant fiber coupler.	16
3-10	Resonant fiber coupler frequency response.	16
3-11	Tracking system test setup.	18
3-12	Measured closed-loop and rejection transfer functions.	19
4-1	Breadboard fiber-based lasercom optical bench.	21
4-2	Breadboard transmitter fiber coupler.	22
4-3	SBS measurement setup.	25
4-4	SBS measurements.	25
4-5	Fiber-based transmitter.	27

LIST OF TABLES

Table No.		Page
3-1	Strawman Receiver Power Loss Budget	9
3-2	Tracking System Parameters	14
4-1	Preliminary Transmitter Fiber Coupler Specifications	23
4-2	Strawman Transmitter Power Loss Budget	27

1. INTRODUCTION

The advantages of fiber optics in ground-based communication systems are widely recognized; however, the utility of fiber optics within free-space optical communication systems is not. Although there has been some discussion of fiber optics within free-space lasercom systems [1,2], most designs do not utilize fiber optics at all [3-10]. The current generation of spaceborne optical communication systems relies on the use of bulk optics, such as mirrors and lenses, rigidly mounted to an optical bench to get light from the optical sources to the exit aperture or from the entrance aperture to the optical receiver. These designs are all very sensitive to thermal and mechanical perturbations as well as to the detailed dynamic characteristics of the host spacecraft [3]. Optical fibers can provide the means to remotely locate the transmitter lasers, local oscillator (LO) lasers (in the case of a coherent system), and the receiver from the front-end optics. This allows flexibility in the mechanical design which can reduce the size, weight, and stability requirements of the optical module.

There are several key issues that must be addressed in successfully utilizing fiber optics in a space-based lasercom package. Among these are efficient source-to-fiber coupling (with low feedback), efficient telescope-to-receiver coupling, and dynamic pointing and tracking. This paper focuses mainly on the issues of pointing, tracking, and receiver communication performance. The design of a fiber-coupled transmitter module will be presented at a later time. Preliminary experimental results of our breadboard fiber-based lasercom system are presented.

We assume the use of a coherent lasercom system, although the results are directly applicable to a direct detection system. Section 2 contains an overview of a fiber-based lasercom system. Section 3 discusses theoretical and experimental results on the communication, tracking, and acquisition subsystems. Section 4 discusses aspects of the transmitter subsystem as well as our breadboard fiber-based lasercom system. Section 5 contains a conclusion and discussion.

2. SYSTEM OVERVIEW

Figure 2-1 shows a strawman optical prescription. One obvious difference between the fiber-based system and the conventional approach is the remotely located transmitter and receiver. Although it is not necessary to remotely locate these items, this important feature allows for a number of advantages. It reduces the number of optical elements, servo mechanisms, and thermal/mechanical interfaces. For instance, relay lens groups are no longer required between the transmitter module and the fast steering mirror, and thermal and mechanical disturbances causing flexing between the transmitter, receiver, and diplexer no longer affect pointing and tracking performance [7].

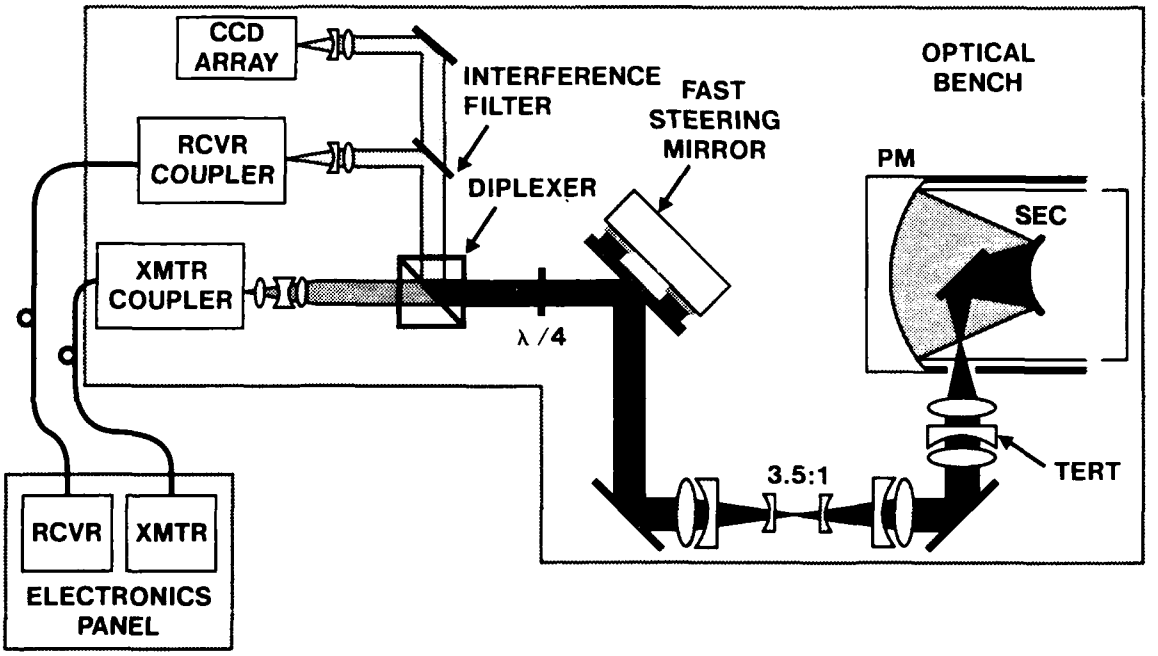

Figure 2-1. Optical schematic.

As in a conventional optical receiver, the incoming circularly polarized light is collected using an optical telescope. To allow for coarse pointing, a gimballed telescope or a fixed telescope and a gimballed flat can be used. In some instances a gimballed telescope allows for lower weight and is shown here. To prevent pupil-walk relay optics are used to image the entrance pupil onto a fast steering mirror. The fast steering mirror is a key element within the spatial tracking system and is used to correct for high frequency platform disturbances. This high bandwidth loop is nested inside a low bandwidth loop, containing the gimballed telescope, which prevents the fast steering mirror from saturating and minimizes off-axis operation (and the

associated optical aberrations) of the telescope. A $\lambda/4$ waveplate converts the incoming circular polarization to linear which can then be separated from the transmitted beam via the polarization diplexer. Prior to the start of communication the spatial uncertainty region must be searched for the transmitting satellite. To accomplish this task a charge-coupled device (CCD) performs a parallel search for the transmitter. Simultaneously the uncertainty region is illuminated by turning on a separate beacon laser or by switching the transmitter laser to a spoiled beam mode [3, 7]. The choice of whether or not to use a separate beacon laser is dependent on the sensitivity to scatter light from the transmitter into the CCD. For some systems the optical isolation of the polarization diplexer alone may not be sufficient. For this and other reasons, it may be beneficial to have two separate transmitters (a beacon and a communication transmitter). The beacon laser frequency is separated from the normal communication laser in order to allow an interference filter to achieve additional isolation. If a high degree of transmit/receive optical isolation is not required then one transmitter laser and a flip mirror instead of an interference filter could be used. Once acquisition is complete the communication signal will be directed to the communication receiver. The received signal is focused directly onto an active fiber coupler containing the receiver single-mode fiber. Using standard nutation tracking techniques, the coupler can provide both tracking and communication information. For coherent systems the polarization-preserving fiber is an attractive approach to maintaining proper mode matching with the subsequent LO field. The transmitter is coupled via a polarization-preserving single-mode fiber to the transmitter coupler which is mounted on the optical bench. The fiber output is collimated and combined with the receive signal in the polarization diplexer. To accomplish the boresight and point-ahead functions, the transmitter coupler has the ability to accurately offset the position of the fiber in the focal plane.

3. NUTATING FIBER RECEIVER

3.1 OVERVIEW

One of the most important features in space-based lasercom systems is the need for a high precision, high bandwidth, large dynamic range spatial tracking system. Many papers have been written on the design and performance of such systems [7-10]. The system proposed here is unique in that it uses a high bandwidth nutation fiber as an angle error sensor. The basic concept is shown in Figure 3-1. In this section we will describe the design and performance of such a system.

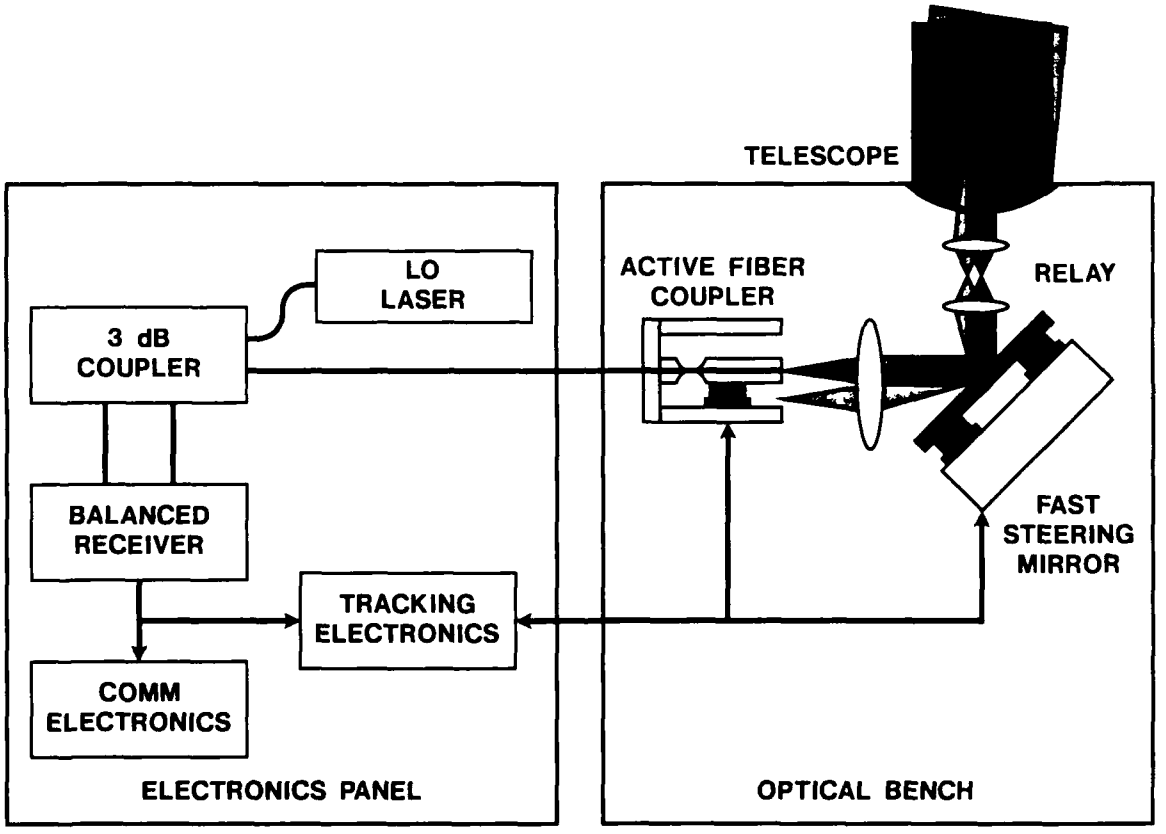

Figure 3-1. Nutating fiber receiver.

The active fiber coupler can be used as a tracking error sensor by employing standard nutation techniques. The key feature of such a system is the small circular scan of the end of the optical fiber which is located in the focal plane of the optical system. As seen in Figure 3-2, if the received beam is accurately tracked the fiber tip is scanned around a constant power contour of the coupling profile. If the received beam is not accurately tracked, the angular offset will result in a displacement from the center of the coupling profile. The resulting periodic change in coupled power as the fiber tip is scanned contains the tracking information. Figure 3-3 illustrates one example of how relatively simple electronics can be used to derive estimates of the tracking error. The tracking error estimates are proportional to the derivative of the coupling profile and are extracted by synchronously detecting the i.f. power. These estimates are then fed back to the FSM to correct for the error. Potentially the need for the fast steering mirror can be eliminated by feeding back directly to the active fiber coupler. There are, however, two reasons for including it. First, it increases dynamic range. Second, the point-ahead and boresight requirements for free-space communication systems are more easily implemented by combining the transmit and receive beams (with the appropriate angular offset) after the fast steering mirror has tracked out the platform disturbances.

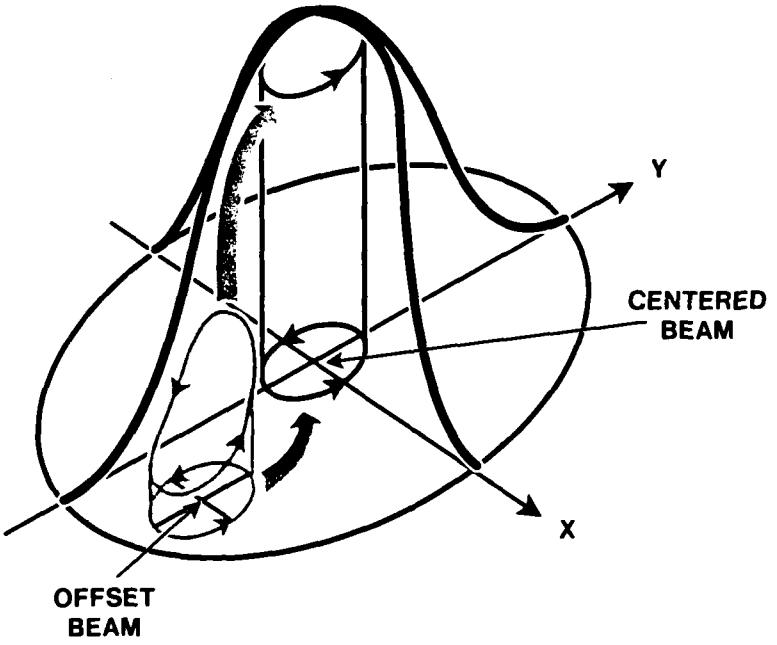

Figure 3-2. Fiber coupling profile.

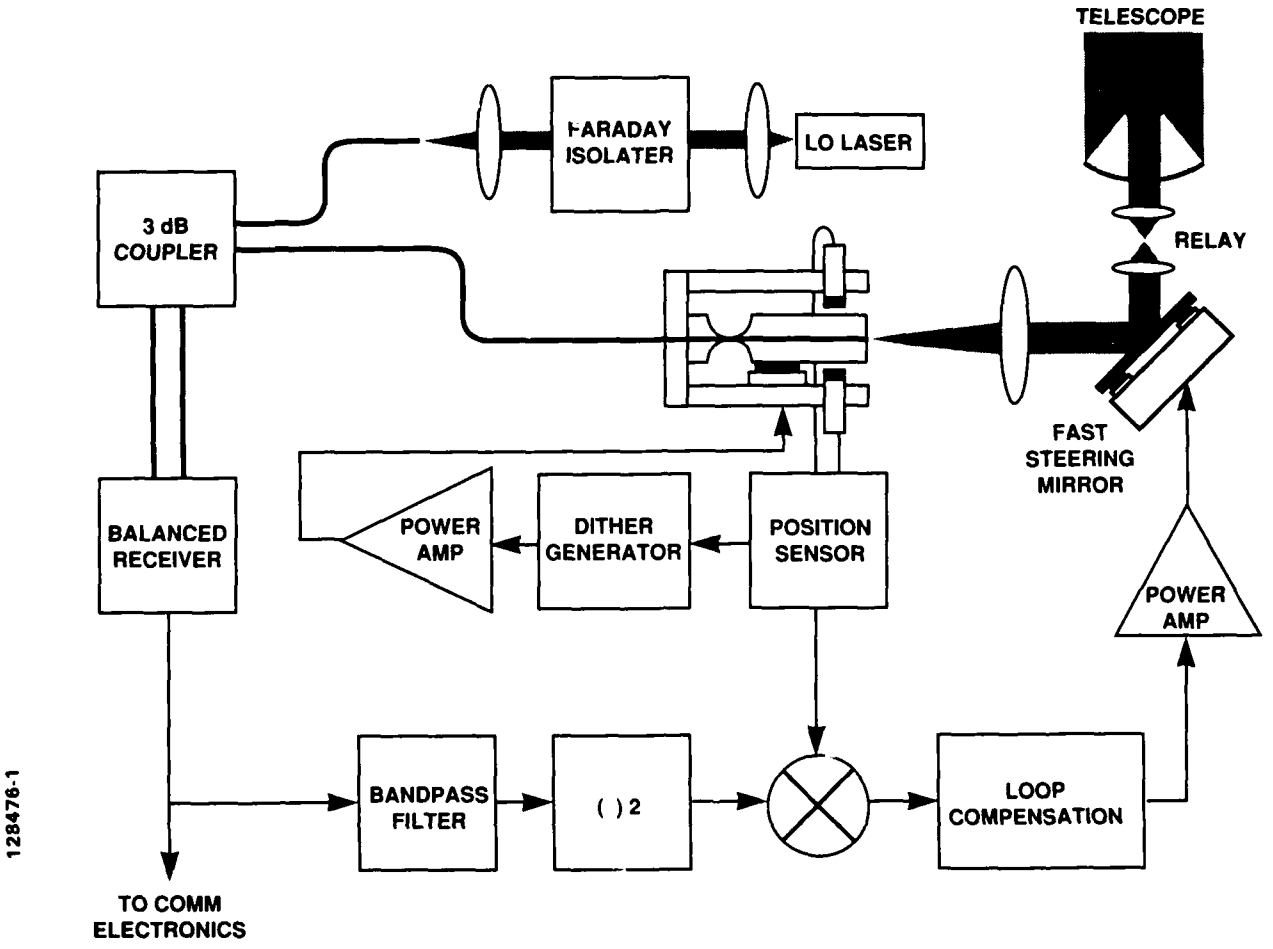

Figure 3-3. Tracking system diagram.

3.2 COMMUNICATION PERFORMANCE

We will now analyze the communication performance of a nutating fiber receiver. A simplified analysis will determine the average communication signal power loss as a function of nutation depth and relative signal beam diameter. The more exact analysis of determining the effect on communication bit-error-rate remains to be completed [11]. Assuming small spatial tracking errors, that the received signal is a plane wave, and that the fiber mode profile is Gaussian [12-14], the average communication signal power loss (derived in the appendix) is given by the square of $m(\phi)$, where

$$m(\phi) = \sqrt{2P_s}\,\frac{d}{\sigma}\int_0^1 dx\; x\; \exp\left[-\left(\frac{dx}{2\sigma}\right)^2\right] J_0\left(\frac{\pi x \phi}{\frac{\lambda}{d}}\right)$$

$$\sigma = \frac{\lambda f}{\pi \sigma_f}$$

where P_s is the total received signal power, d is the signal field diameter, ϕ is the nutation depth, σ is the equivalent 1/e amplitude radius of the fiber mode profile after transformation by the focusing lens, λ is the signal wavelength, f is the focusing lens focal length, and σ_f is the fiber 1/e amplitude radius.

The maximum signal power that can be coupled into the optical fiber is limited due to the spatial dissimilarity of the plane wave (or equivalently the Airy disc) and Gaussian profiles. Figure 3-4 shows the loss in communication performance as a function of d/σ and ϕ. In this and subsequent plots ϕ has been normalized by the full-width-half-maximum beamwidth (BW). Note that 1 BW is approximately equal to λ/d. Loss is defined as the increase in signal power that is required to achieve optimal performance. A *minimum communication* loss of 0.9 dB occurs at $\phi = 0$ and $d/\sigma = 2.2$. This is the fundamental loss to the mode mismatch. As shown in the figure, the dither signal imposed on the fiber tip adds additional loss. Note that for $\phi \leq 0.5$ BW the optimum d/σ remains ~2.2.

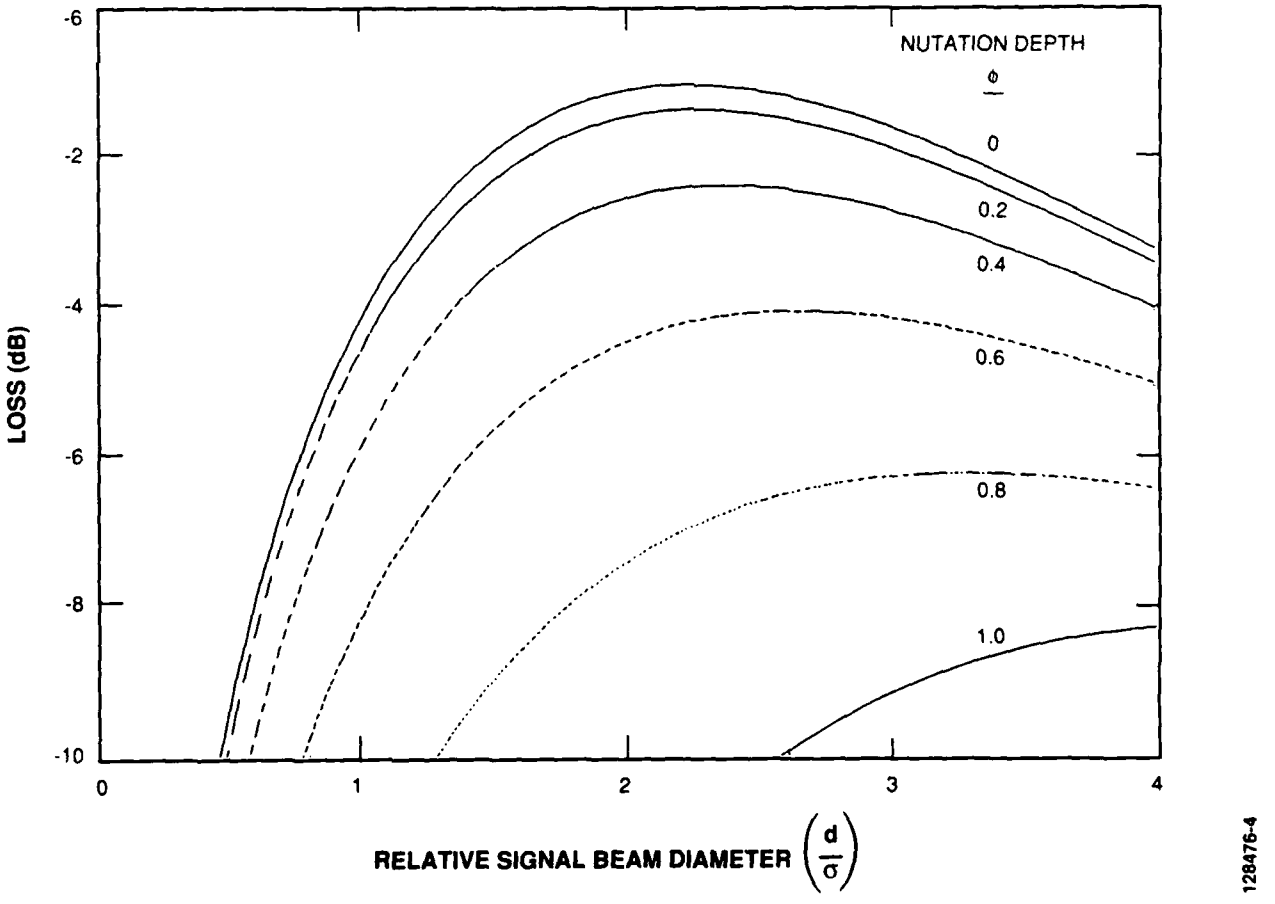

Figure 3-4. Communication channel loss vs relative signal beam diameter and nutation depth.

There are a number of additional losses to be considered in an actual nutating fiber receiver. Table 3-1 contains a strawman receiver loss budget. This table is based on experimental measurements and detailed experience obtained from the LITE program [3,7]. The telescope obscuration loss is calculated as in [15-17]. The bulk optical throughput loss includes effects of scattering and absorption from the telescope entrance aperture to the focusing lens on the receiver fiber coupler. The calculated loss is derived from data used in the LITE study. A worst-case polarization error of 30 deg (15 deg for transmit and receive) is assumed and is also a result of the LITE study. It represents the power that is lost at the diplexer due to elliptical rather than circular polarization incident on the $\lambda/4$ waveplate. The effect of received signal phase distortion is calculated as a Strehl ratio. Note that the LO phase-front distortion does not contribute to mode matching loss as in a conventional heterodyne receiver [18]. The receiver pupil-walk is an allocated number that can be met with straightforward FSM and relay-lens design. The free-space-to-fiber coupling and nutation loss were previously described. The 3-dB fiber coupler, Fresnel reflection, attenuation, and fiber extinction ratio are all within the present capabilities of optical fibers. Note that the effects of radiation on fiber attenuation has not been taken into account.

The loss of the fiber-based receiver (5.8 dB) compares well with the loss calculated from the preliminary LITE heterodyne receiver design (5.2 dB) which used a bulk optics approach.

TABLE 3-1

Strawman Receiver Power Loss Budget

Telescope Obscuration (15% Central + 10% Spiders)	–0.1
Bulk Optical Throughput	–1.1
Polarization Error (XMTR + RCVR = 30 °)	–0.1
Received Signal Phase Distortion ($\lambda/15$)	–0.8
LO Phase Distortion	–0.0
Receiver Pupil-Walk	–0.1
Free-Space-to-Fiber Coupling (d/σ = 2.2)	–0.9
Nutation Loss (ϕ = 0.36 BW)	–1.1
3-dB Fiber Coupler Loss	–0.2
Reflection from AR-Coated Fiber Facets (each 98%)	–0.2
Attenuation in Fiber	~0.0
Fiber Polarization Extinction Ratio (15 dB for LO and Sig)	–0.3
Quantum Efficiency	–1.0
Total	-5.8 dB

3.3 NOISE EQUIVALENT SPECTRAL DENSITY

As shown in Equation (1), the two main components of the system tracking error present in each angular axis are the uncompensated tracking error (σ_{uc}) and the noise induced tracking error or noise equivalent angle (NEA) [8]. In this section we will discuss the NEA and in section 3.5 the uncompensated tracking error will be discussed.

$$\sigma_T^2 = \sigma_{uc}^2 + NEA^2 \tag{1}$$

This single-axis NEA is related to the (single-sided) noise equivalent spectral density (NESD) and the noise equivalent bandwidth (NEB) of the tracking loop by [8]

$$NEA = \sqrt{NESD\, NEB}$$

A simplified analysis will determine the NESD as a function of nutation depth and relative signal beam diameter. Under the same assumptions described in section 3.2 and in addition assuming the tracking information is derived by non-coherent (square-law) detection of the i.f. heterodyne signal and subsequent synchronous demodulation of the nutation signals (see Figure 3-3), the NESD of the tracking system is given by (derived in the appendix)

$$NESD = \frac{1}{\frac{\eta K(\phi)^2}{h\nu}} \left[1 + \frac{1}{2} \frac{W}{\frac{\eta m(\phi)^2}{h\nu}} \right]$$

$$K(\phi) = \frac{\sqrt{P_s}\, \pi \frac{d}{\sigma} \int_0^1 dx\, x^2 \exp\left[-\left(\frac{dx}{2\sigma}\right)^2 \right] J_1\left(\frac{\pi x \phi}{\frac{\lambda}{d}}\right)}{\frac{\lambda}{d}}$$

where W is the noise bandwidth of the i.f. filter preceding the square-law detector, h is Planck's constant, ν is the optical frequency, and η is the detector quantum efficiency. It can be shown that the term in brackets is a penalty due to non-coherent detection of the heterodyne i.f. frequency and thus the result for coherent detection is obtained by setting W = 0. The second term inside the square brackets can be interpreted as the i.f. signal-to-noise ratio (SNR). Therefore for large SNR the rms noise performance is equivalent to the case where coherent detection is used.

In order to analyze tracking performance the NESD for the nutating fiber receiver will be compared to the NESD bound derived in [9]. This bound, which will be used when SNR>>1, is given by

$$NESD_H = \left[\frac{\eta P_s}{h\nu} \frac{\pi^2}{4} \frac{1}{\left(\frac{\lambda}{d}\right)^2} \right]^{-1} \qquad SNR>>1 \tag{2}$$

For low SNR<<1, the comparison will be made (somewhat arbitrarily) assuming the above bound is achieved with an additional loss due to non-coherent detection, i.e.,

$$NESD_L = \frac{1}{\frac{\eta P_s}{h\nu}\frac{\pi^2}{4}\frac{1}{(\frac{\lambda}{d})^2}}[\,1+\frac{1}{2}\frac{W}{\frac{\eta P_s}{h\nu}}\,] \qquad SNR<<1$$

For large SNR>>1 the tracking performance is dependent on $K(\phi)^2$; for SNR<<1 the tracking performance is dependent on $m(\phi)K(\phi)$. Figures 3-5 and 3-6 show the relative tracking performance loss (with respect to the bounds) as a function of d/σ and ϕ for a plane wave signal. These losses are also interpreted as the increase in signal power that is required to achieve the performance bound. For SNR>>1 minimum tracking loss of 7.9 dB occurs at $\phi = 0.78$ BW and $d/\sigma = 1.92$. Note that below $\phi = 0.8$ the optimum d/σ remains near 1.84. While for SNR<<1 the minimum tracking loss of 6.3 dB occurs at $\phi = 0.52$ BW and $d/\sigma = 2.08$.

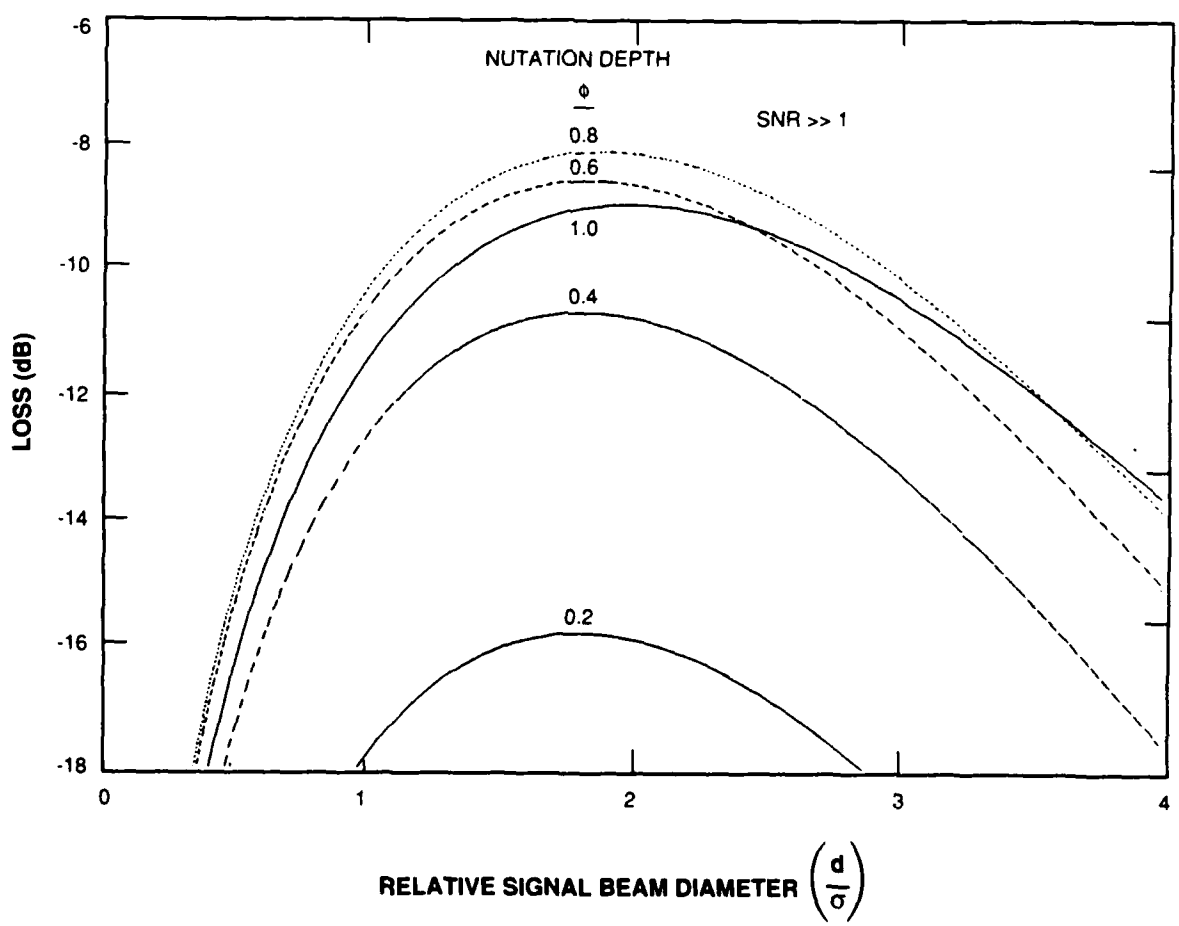

Figure 3-5. Tracking channel loss vs relative signal beam diameter and nutation depth (SNR>>1).

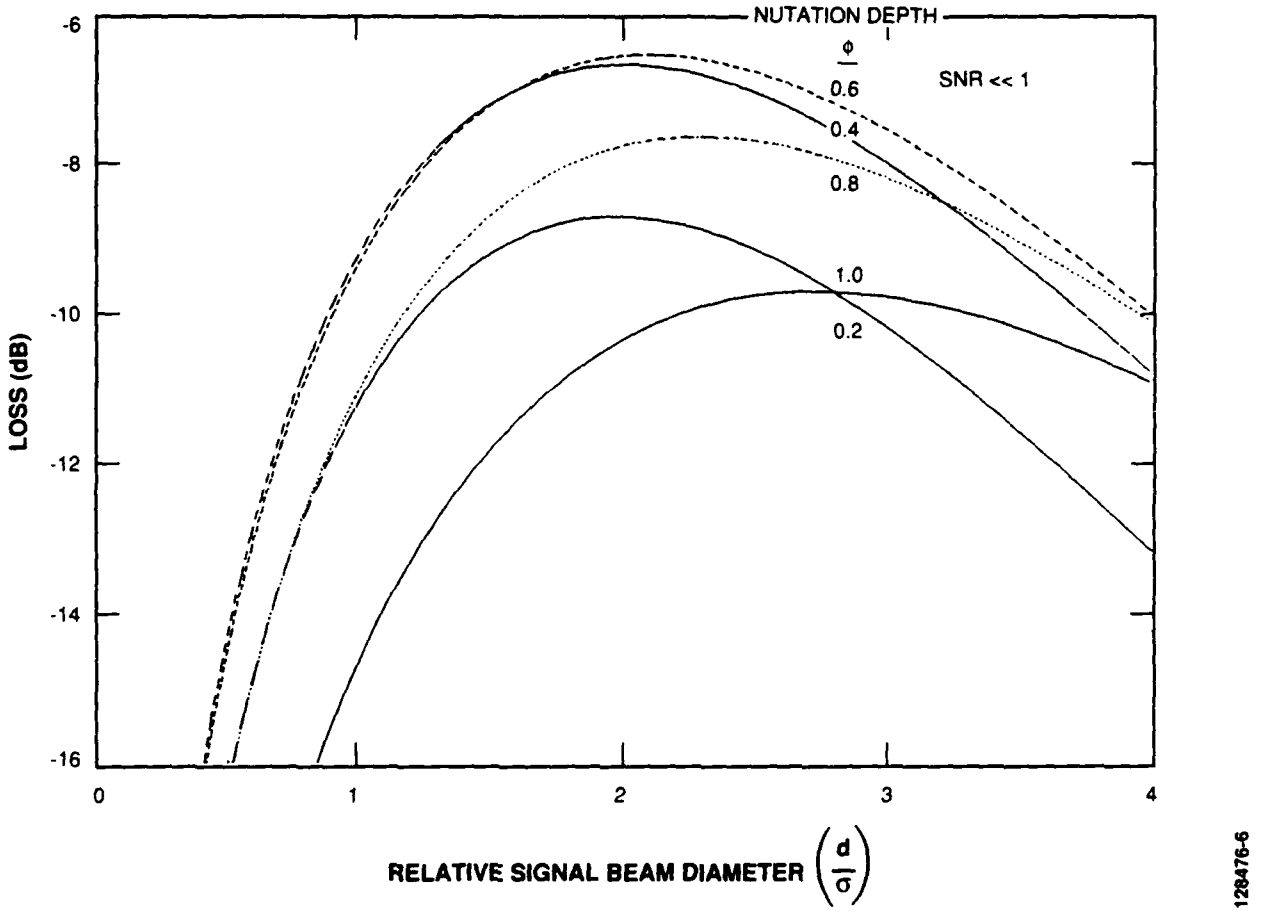

Figure 3-6. Tracking channel loss vs relative signal beam diameter and nutation depth (SNR<<1).

In the interest of minimizing communication performance loss (loss < 2 dB) the best tracking performance is obtained at ~$d/\sigma = 2.2$. Figure 3-7 shows the resulting communication and tracking losses as a function of nutation depth. In subsequent analyses we will assume a nutation depth of 0.36 BW which results in $m(0.36) = 0.792$ (communication loss of 2 dB) and $K(0.36) = 0.413$.

We will now calculate the required signal power to achieve acceptable tracking performance. Typically optical systems require angular stabilization to a fraction of an antenna beamwidth [7,11]. To achieve sufficient rejection of typical spacecraft platform disturbances, an open-loop crossover frequency of ~1 kHz is required. (The corresponding closed-loop NEB is ~ 3.5 kHz.) In this paper we will assume an NEA of 0.05 BW per angular axis rms tracking error is acceptable. Figure 3-8 shows the signal power required to achieve an NEA of 0.05 BW for an ideal optical receiver (no implementation losses). An additional loss of

~ 3.8 dB would be encountered in an actual system (see Table 3-1 entries minus free-space-to-fiber coupling and nutation losses). The figure contains the performance for the expected mode of non-coherent detection. In addition, the coherent detection (SNR>>1) and tracking bound [Equation (2)] are included for comparison. Table 3-2 lists the parameters assumed in the calculation. A signal power of 2.9 x 10^8 p/s is required to meet a 0.05 BW NEA per angular axis.

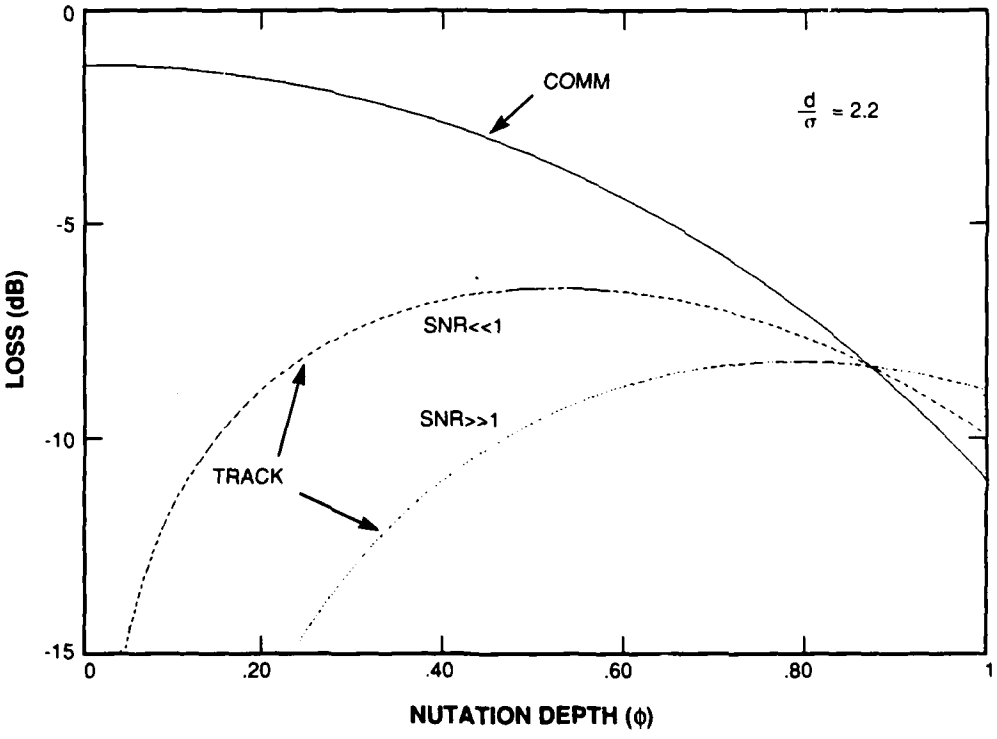

128476-8

Figure 3-7. Communication and tracking loss vs nutation depth.

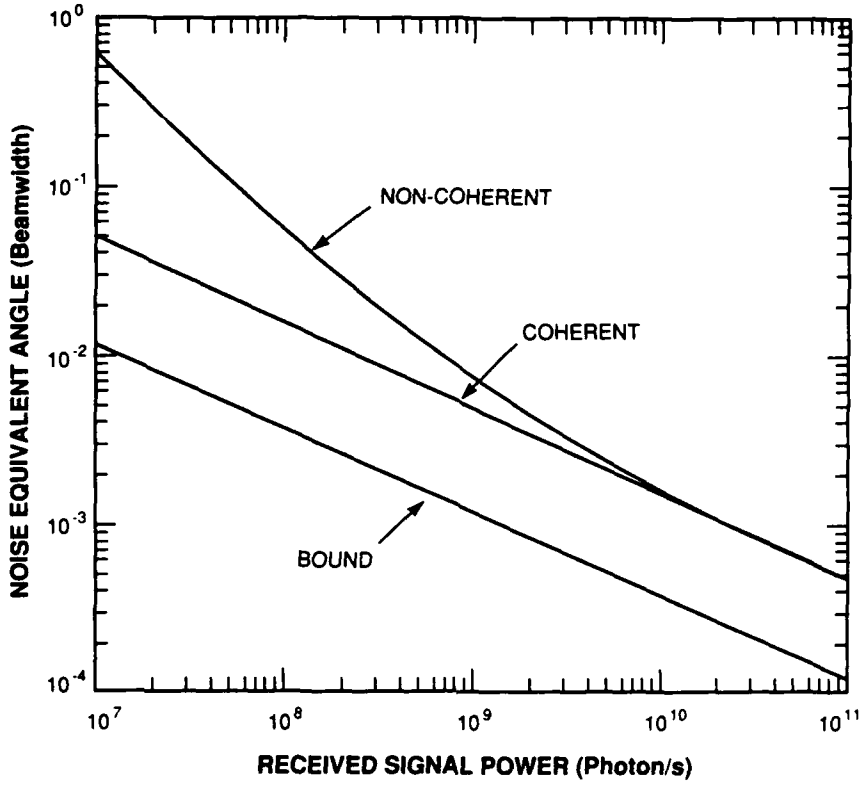

Figure 3-8. NEA vs signal power.

TABLE 3-2

Tracking System Parameters

λ	Signal Wavelength	0.86 μm
ϕ	Nutation Depth	0.36 BW
$m(\phi)$	Comm Coupling Coefficient	0.792
$K(\phi)$	Tracking Discriminator Gain	0.413 BW^{-1}
f_o	Open-Loop Crossover Frequency	1000 Hz
NEB	Tracking Loop Noise Equivalent Bandwidth	3500 Hz
W	I.F. Predetection Noise Bandwidth	1.3 GHz
η	Quantum Efficiency	0.8
Required Signal Power for 0.05 BW NEA (Ideal)		1.2×10^{8} p/s
Required Signal Power for 0.05 BW NEA (Strawman)		2.9×10^{8} p/s

3.4 RESONANT FIBER COUPLER

One of the key elements in the nutating fiber receiver is the active fiber coupler. Nutating fiber devices have been built before [19]. However, there are some unique requirements for a space-based system. As previously mentioned, typical spacecraft platforms dictate that the spatial tracking system have an open-loop crossover frequency of ~ 1 kHz. To support this bandwidth requires a nutation frequency of ~ 10 kHz. As discussed in section 3.3 a nutation depth of ~ 0.36 BW is desirable. Assuming single-mode 0.86-μm step-index fiber with a core radius of 2.5 μm and a V-number of 2, then the 1/e amplitude radius is $\sigma_f = 3.175$ μm. Assuming $d/\sigma = 2.2$, then ± 0.36 BW corresponds to $\pm 0.36\,(\pi/2.2)\,\sigma_f = \pm 1.6$ μm of required dynamic range [12-13]. In addition to these requirements are the usual requirements for space systems: small, lightweight, rugged, stable, low power, etc.

One of the important elements within the active fiber coupler are the actuators. One candidate is a piezoelectric translator (PZT). However, PZTs require high voltage drives (150 to 1000 V) and have reliability considerations. A more attractive alternative is to use a linear electromagnetic "voice coil" actuator. These are inexpensive, small, and can be driven from standard analog components and supplies. However, most voice coil actuators do not have enough force to move their own mass the required few micrometers at these high speeds. To circumvent this limitation we have developed a resonant fiber coupler.

An earlier version of this device is depicted in Figure 3-9. Two orthogonally mounted moving voice coils are mounted on a mechanical flexure. A microcapillary holding the optical fiber is mounted inside the center of the flexure. The flexure is designed so that after the loading of the actuator coils its resonant frequency is at the desired nutation frequency. By driving the flexure at its resonance there is a large mechanical advantage limited only by the residual mechanical damping. Figure 3-10 shows some results from an early prototype. Note that over 30 dB of gain is obtained. The maximum dc range of the present design is ~ $\pm$ 60 nm which would result in over 2 μm of motion when driven at the resonant frequency of ~ 9 kHz. More recently a resonant fiber coupler has been fabricated with a resonant frequency of ~13 kHz.

Two "eddy current" sensors are mounted apposed to the actuators to provide positioning information. Each is mounted to view the side of the flexure that is opposite each actuator. The main purpose of these sensors is to ensure accurate demodulation of the i.f. signals that contain tracking errors. In addition, these position sensor signals can be fed back to an active dither generator which will ensure that the drive signals track the resonant frequency of the flexure, the proper nutation depth is achieved, and the scan is circular.

The resulting design for the resonant fiber coupler meets most of the requirements for our application. It is simple, small, lightweight, and rugged. When the nutating fiber receiver is compared to the more conventional bulk optics approach, it becomes clear that the resonant fiber coupler replaces many times with size and weight in equivalent bulk optics. We are presently working on an improved design to further reduce the weight as well as increase the range, resonant frequency, and reliability for space use.

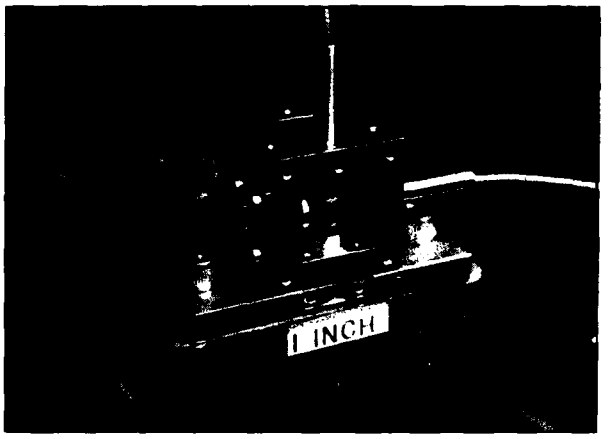

128476-9

Figure 3-9. Breadboard resonant fiber coupler.

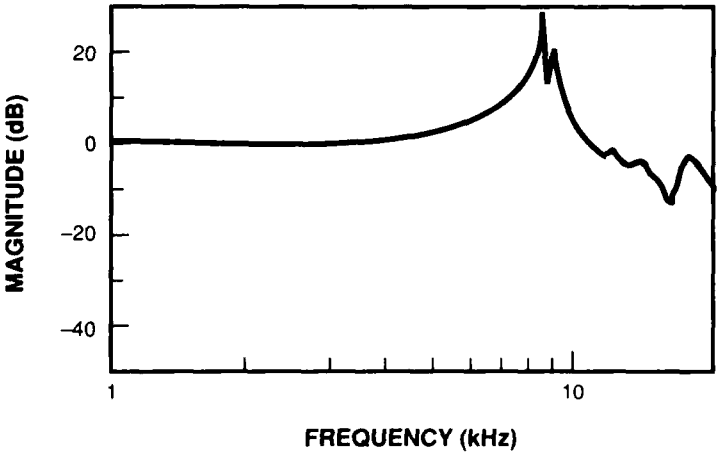

125489-9

Figure 3-10. Resonant fiber coupler frequency response.

3.5 TRACKING LOOP REJECTION

The uncompensated tracking error is governed by the tracking loop rejection, R(f), and the angular disturbances spectrum, $S_\theta(f)$, as shown in Equation (3) [8]

$$\sigma_{uc}^2 = \int_{-\infty}^{\infty} |R(f)|^2 S_\theta(f)\, df \tag{3}$$

The rejection is related to the closed-loop transfer function, H(f), by

$$R(f) = 1 - H(f)$$

The test setup shown in Figure 3-11 was used to determine if the nutating fiber receiver concept could meet the tracking system rejection requirements. The light incident onto the two-axis disturbance FSM was a uniform intensity ~10-mm diameter beam. Simulated spacecraft platform disturbances as well as sinusoidal disturbances were introduced using the disturbance FSM. The disturbance mirrors had internal angular position sensors so that the disturbance input could be accurately determined. The reflected beam was then directed onto a 5-mm aperture stop simulating the telescope aperture and then onto the two-axis tracking FSM. The focusing lens was sized to yield $d/\sigma \approx 2.2$. The signal was combined with the LO using a single-mode polarization-preserving 3-dB fiber coupler. Both the signal and LO lasers were 30-mW GaAlAs semiconductor diode lasers with output wavelengths of 0.86 μm. Using a bulk optics approach, ~ 5 mW of LO power was easily coupled into the optical fiber using a collimating lens, anamphoric prism pair (to circularized the beam), a Faraday isolator, and a focusing lens. Isolation issues are further discussed in section 4.3.

Azimuth and elevation error estimates were output from the angle error detector. By measuring the transfer function between the disturbance position sensors and the angle error detector outputs, both the rejection and closed-loop transfer functions were obtained. Figure 3-12 shows the measured results. The compensator was designed to have a 500-Hz crossover frequency. Its design as well as many of the other components are similar to those described in [8]. The resulting tracking system rejection is adequate to track out the angular disturbances encountered on many spacecraft platforms to a 0.05-BW uncompensated tracking error.

3.6 ACQUISITION

The advantages of a CCD-based parallel acquisition system over other approaches such as scanning and zooming are well known [35, 36]. Using commercially available CCDs and processing electronics, we have performance spatial acquisition tests. A two-axis beam steering mirror was used to simulate the spatial uncertainty zone. The angle of incidence was stepped in a raster scan pattern over a 200 BW × 300 BW (of a possible 400 BW × 500 BW) field-of-view. At each step the spatial acquisition process was performed and the estimated incidence angle was compared to the actual incidence angle. At a received (incident) signal power of $\sim 3 \times 10^5$ p/s and with an integration time of 1 s the probability of successful acquisition was 0.994 and the rms estimation error was ~0.4 BW. Note that we expect with some simple modifications reliable operation at lower signal powers will be achieved over wider uncertainty zones.

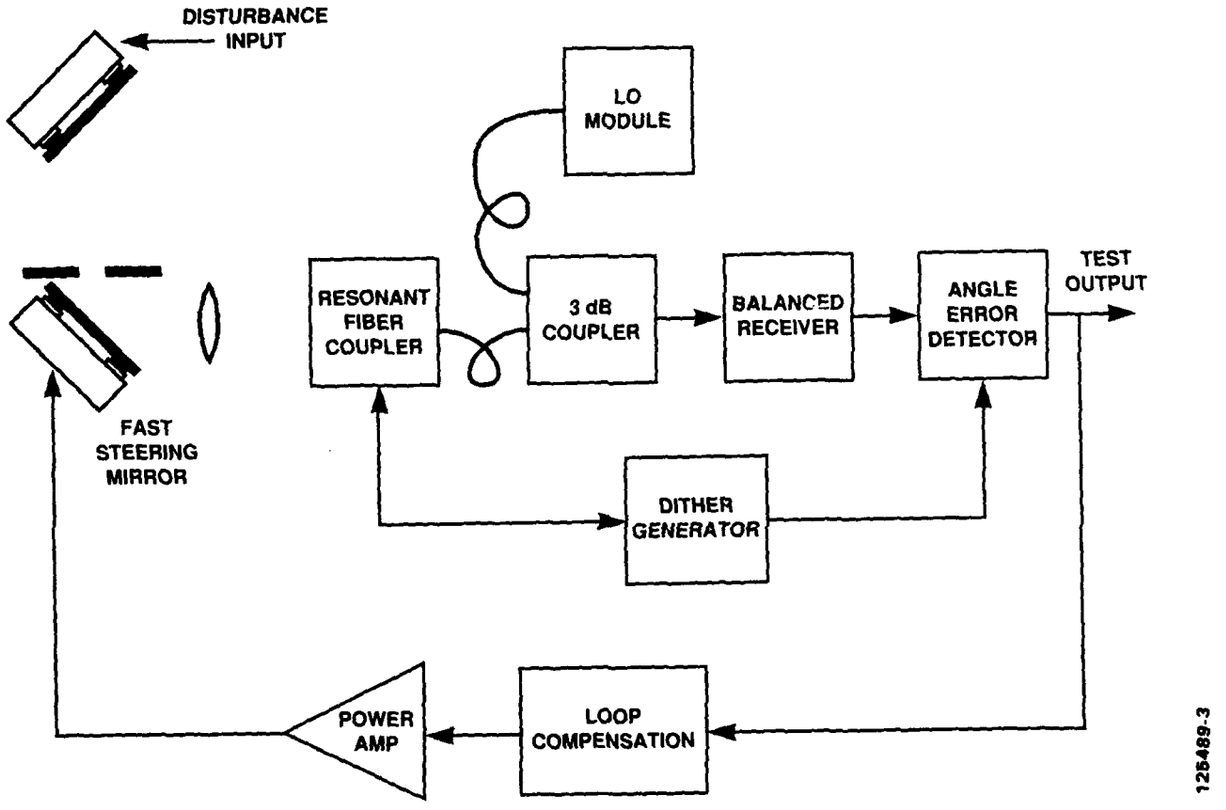

Figure 3-11. Tracking system test setup.

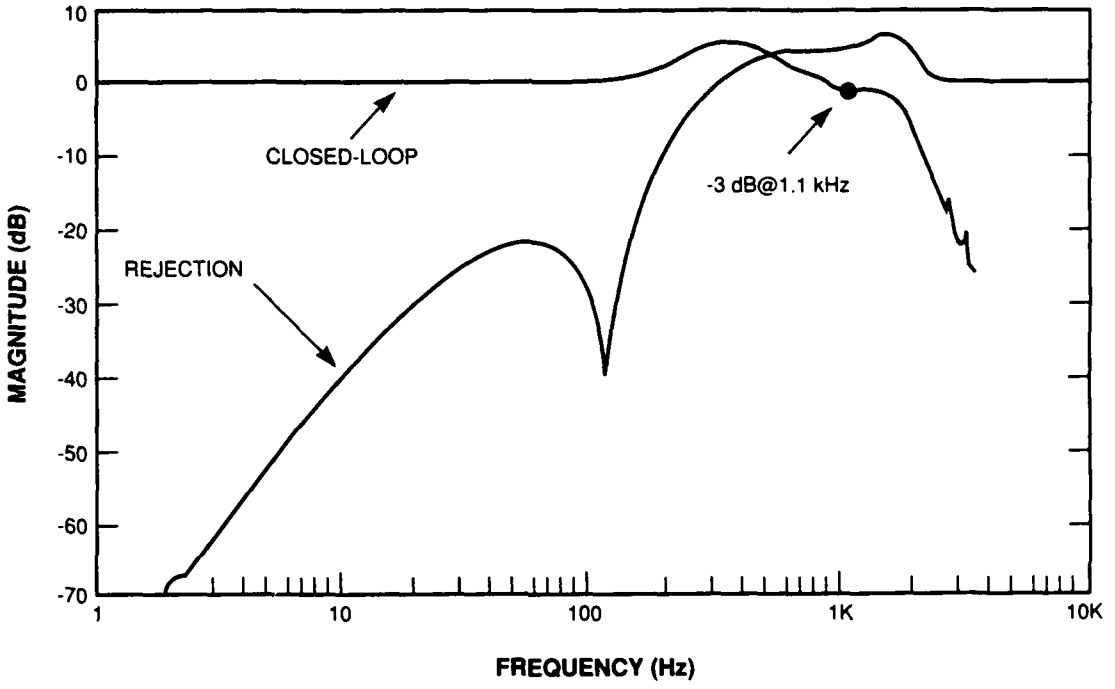

125489-10

Figure 3-12. Measured closed-loop and rejection transfer functions.

4. TRANSMITTER

4.1 OVERVIEW

Figure 4-1 shows our breadboard optical bench containing the transmitter and receiver active fiber couplers, diplexer, two-axis FSM, and a CCD. One key element required in an actual system but missing from the breadboard is the gimballed telescope. The optical bench has an area of 8 × 12 inches. No attempt was made to miniaturize this bench, and it is expected that when an attempt is made that the size may be reduced by as much as a factor of 2. Preliminary testing has demonstrated the ability of this breadboard optical bench to achieve acquisition, high bandwidth tracking, transmitter pointing stabilization, and point-ahead capabilities. We are presently working on an upgraded version which will undergo more quantitative testing.

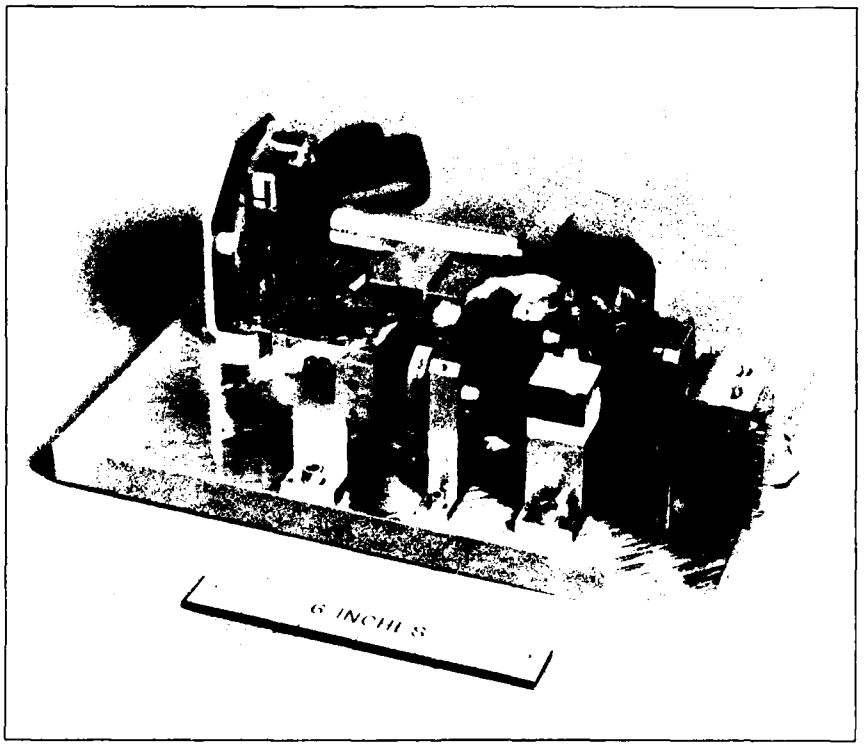

128476-10

Figure 4-1. Breadboard fiber-based lasercom optical bench.

4.2 TRANSMITTER FIBER COUPLER

One of the key elements in the fiber-based lasercom system is the transmitter fiber coupler. It must perform the boresight and point-ahead functions. The design of the transmitter coupler is similar to the receiver coupler in that a fiber is held inside a flexural pivot which is driven by linear electromagnetic actuators and whose position is sensed by "eddy-current" sensors. There are three important differences: it requires lower bandwidth, larger dynamic range, and higher positioning accuracy. Figure 4-2 shows a photograph of the breadboard transmitter fiber coupler.

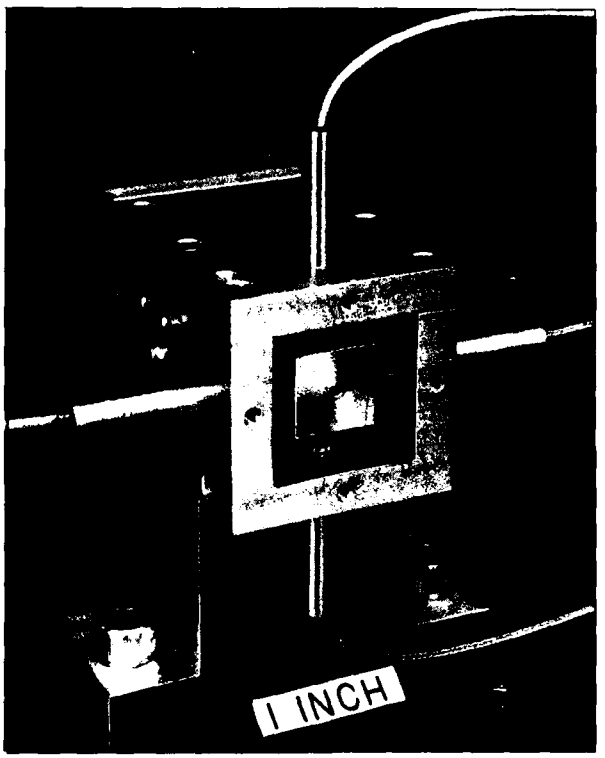

128476-11

Figure 4-2. Breadboard transmitter fiber coupler.

A bandwidth of ~10 Hz is more than sufficient to keep pace with the rate of change in the required point-ahead angle. The dynamic range is dictated by that needed for boresight plus that needed for point-ahead. The boresight function is required in order to compensate for misalignments due to launch loads and on-orbit thermal and mechanical disturbances. Boresight is accomplished by either flipping a retroreflector into the transmitted beam after the $\lambda/4$ waveplate [3,7], or by directing the coarse pointing device to a retroreflector located external to the optical system. The reflected light from the retroreflector (now with the opposite sense

of polarization) is directed onto the receiver fiber coupler. Using either direct detection or heterodyne detection, the transmitter fiber coupler can be displaced until the power into the receiver coupler is maximized. Due to the close proximity of the transmitter and receiver fiber couplers and the short optical path between the couplers, a dynamic range of ± 5 BW should be sufficient to accomplish the boresight function.

The required point-ahead angle is approximately equal to the differential tangential velocity between the two satellites divided by the speed of light [6,7]. A point-ahead angle of ~ 52 μrad is sufficient to handle Earth-to-GEO, GEO-to-GEO and most LEO-to-GEO links. Assuming an antenna beamwidth of 4 μrad, the resulting dynamic range requirement is ±13 BW. Therefore the total required dynamic range is ±18 BW. Assuming single-mode 0.86-μm step index fiber operating with a core radius of 2.5 μm and a V-number of 2, then the 1/e amplitude radius is $\sigma_f = 3.175$ μm [12-14]. Assuming $d/\sigma = 2.2$, then ±18 BW corresponds to $\pm 18\ (\pi/2.2)\ \sigma_f = \pm 82$ μm of required dynamic range.

In order to achieve redundant laser transmitters, it may be desirable to have the transmitter fiber coupler hold more than one fiber core. Under such circumstances the dynamic range of the transmitter fiber coupler would have to be further increased to accommodate the core-to-core separation. To minimize this separation the excess cladding of each fiber could be removed by polishing, a D-core fiber could be used, or multicore fibers could be used [32].

In order to ensure that the point-ahead angle is accurately implemented high precision position sensors are needed on the transmitter fiber coupler. High dc stability is needed to ensure the boresight position is accurately maintained. High precision and repeatability are also needed to ensure that the proper point-ahead displacement from boresight is achieved.

Table 4-1 lists the measured and estimated performance of our breadboard transmitter fiber coupler. We are presently working on an improved design that will increase the dynamic range. This design includes reducing the flexural stiffness and may also include two pairs of actuators operating in push-pull. The estimated accuracy of 0.51 μm rss corresponds to a contribution of ~ 0.11 BW to the total pointing error.

TABLE 4-1

Preliminary Transmitter Fiber Coupler Specifications

Bandwidth	> 10 Hz
Primary Resonance	200 Hz
Dynamic Range	± 20 μm
Power (Maximum)	< 1.6 W
Stability	< 0.1* μm/day
Repeatability	< 0.5* μm
Jitter	< 0.01* μm
Size	1x1x2 in^3

* Estimated

4.3 TRANSMITTER MODULE

The design of the transmitter module is one of the most difficult subassemblies due to the high coupling efficiency, low feedback, and redundancy requirements. High coupling efficiency is difficult to achieve due to the tight tolerances on translation, focus, and tilt between the fiber facet and the beam waist [12,20]. For a single-mode fiber at 0.83 μm, a 1-dB coupling loss can result from a 1.6-μm displacement, a 45-μm focus error, or a 2.2-deg angular offset between the fiber core and the beam waist. Although in some cases the use of up-tapers can help minimize alignment sensitivity, high coupling efficiency is still difficult to achieve [21]. An unfortunate consequence of maintaining high coupling efficiency is the associated high sensitivity to feedback. In order to minimize the effects of feedback to the transmitter laser, over 60 dB of isolation is required [22]. Although optical fibers are remarkable for their low loss and moreover a short length of this low loss fiber (< 5 m) is used, the Rayleigh scattering and other scattering mechanisms in the core and cladding dictate the need for an optical isolator [23-25]. Fresnel reflections from the input and exit fiber facets can effectively be minimized by polishing the fiber facets on an angle and AR coating [26, 27]. In the 1.3- to 1.55-μm wavelength region efficient high performance compact isolators exist and are directly applicable to this problem. In fact miniature laser modules are commercially available that contain a laser, thermal electric cooler, optical isolator, and fiber pigtail. However, in the 0.83-μm region Faraday isolators tend to be heavy and bulky. This fact tends to make a multiple isolator approach associated with laser redundancy less attractive. In our breadboard, packaging issues and redundancy of a 0.83-μm laser transmitter module have not yet been addressed. We used a bulk optics approach containing a 30-mW GaAlAs laser operating at 0.86 μm, housed in a temperature controller, the output of which was collimated, circularized, and directed through a Faraday isolator and focused into a polarization-preserving optical fiber in the preliminary experiments discussed here.

As transmitter powers become large nonlinear behavior within the fiber medium becomes an important design consideration. Nonlinear effects can limit the maximum power delivered by the optical fiber, contribute to optical feedback, and damage the optical fiber. Typically, for narrow linewidth lasers, the nonlinear mechanism with the lowest threshold power is stimulated brillouin scattering (SBS) [28-31]. The threshold power is dependent on a number of parameters such as fiber length, wavelength, core diameter, and laser linewidth. For a 13.6-km length of 1.3-μm fiber, experiments have shown that SBS can limit the maximum fiber output power to < 2 mW [30]. As shown in Figures 4-3 and 4-4 we have performed a similar experiment at 0.86 μm on a 2.2-km length of Corning Flexcore 850 single-mode fiber. Note that in Figure 4-3 the input, reflected, and transmitted power correspond to the appropriate values inside the optical fiber. The theoretical threshold power for this configuration was ~13 mW. Note that this value agrees well with the experimental measurements. Extrapolating these results to a 5-m length of polarization maintaining fiber yields a threshold power of 1.5 W. Until laser transmitter output powers exceed this value, SBS will not be a limiting factor in a fiber-based transmitter.

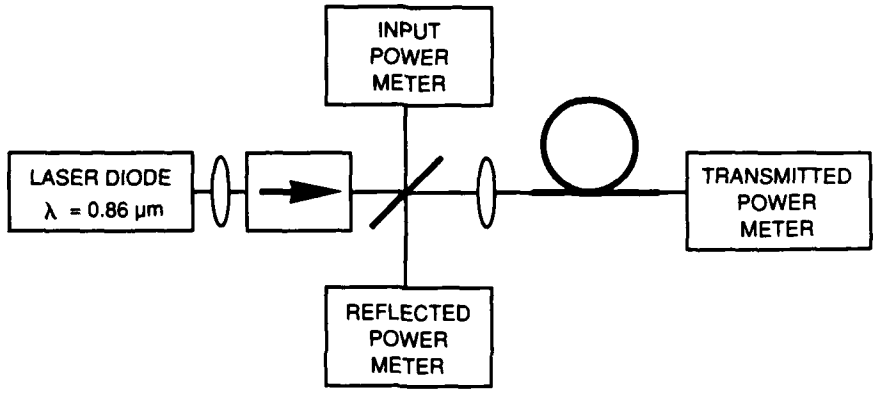

136254-3

Figure 4-3. SBS measurement setup

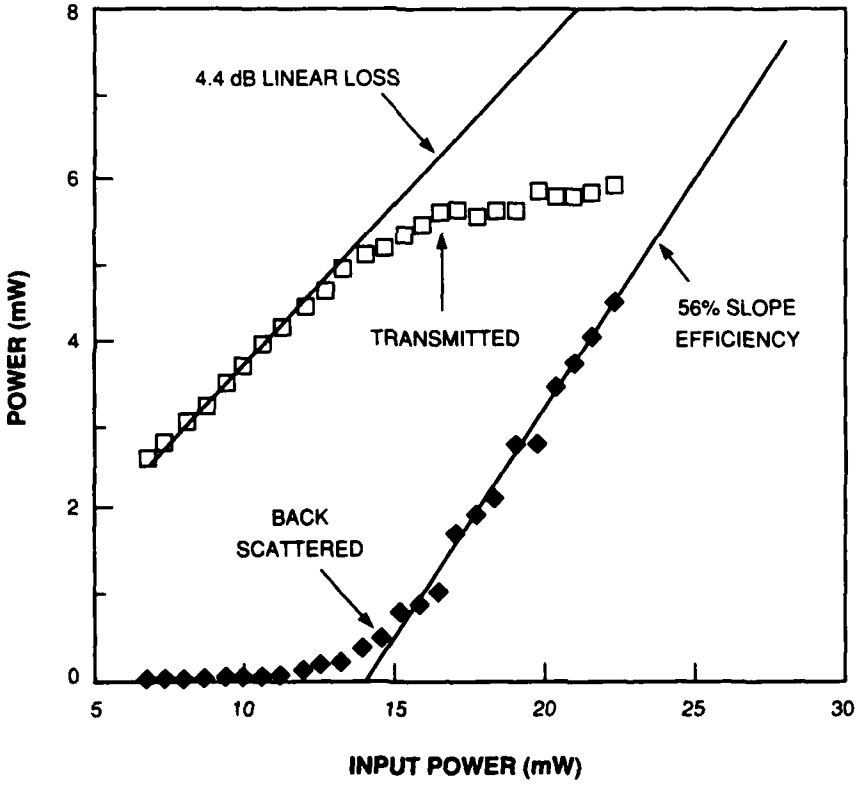

136254-2

Figure 4-4. SBS measurements

4.4 STRAWMAN TRANSMITTER POWER LOSS BUDGET

Table 4-2 contains a strawman transmitter loss budget. Figure 4-5 contains a simplified optical schematic for the assumed transmitter design. The lasers are collimated, circularized using anamorphic prism pairs, sent through an optical isolator and focused into a polarization-preserving optical fiber. Redundancy is provided by nesting the cores of two (or more) fibers close together within the transmitter fiber coupler. Although this increases the required dynamic range of the transmitter fiber coupler by a few beamwidths over that stated in section 4.2, it is more efficient than some other alternatives such as using a 2:1 fiber switch.

The collimation, shaping, and focusing throughput losses as well as the signal phase distortion are based on the MIT/LL transmitter module [33]. The isolator throughput loss is based on typical commercially available devices. The estimated spatial mode mismatch loss is a result of truncation losses in the collimation lens and isolator, pupil-walk between the laser and the input fiber facet, and the fact that the laser and fiber mode profiles are only approximately Gaussian [12-14,34]. The bulk optics throughput loss results from imperfect AR coating, reflection, and absorption between the transmitter fiber coupler and the optical window. Its value is derived from the LITE study. The obscuration and truncation loss are calculated as in [15-17]. And finally the wavefront quality of $\lambda/15$, calculated as a Strehl ratio, and the beamwalk are based on the LITE system [3,7,33].

Note that in our breadboard transmitter we have measured the throughput efficiency from the output of the laser to the output of the single-mode fiber to be as low as 1.4 dB. This exceeds the budgeted 2.0 dB in Table 4-2 by 0.6 dB. The 30-dB optical isolater was found to provide marginal performance, and in future designs we may use two isolaters to provide > 60 dB. We expect that in going from a laboratory design to a flight design may use some or all of the 0.6 dB margin.

The loss of the strawman fiber-based transmitter (5.6 dB) is ~ 0.8 dB higher than that loss associated with the bulk optics approach used in the LITE program (4.8 dB). There are many areas in which the loss of the fiber-based transmitter could be improved upon. Implicitly assumed in the strawman system shown in Figure 4-3 is that the laser is directly modulated. One of the advantages of the optical fiber approach is that the wide variety of optical fiber components, both active and passive, can easily be incorporated. For instance, a fiber switch (instead of the multiple core technique to achieve redundancy) followed by a fiber pigtailed external modulator and laser amplifier might be an attractive approach for high-speed high-power applications. This is particularly true at 1.3 and 1.55 μm where these are commercially available devices.

TABLE 4-2

Strawman Transmitter Power Loss Budget

Collimator Lens, Anamorphic Prism Pair, Focusing Lens Throughput	–0.6
Signal Phase Distortion (λ/20)	–0.4
Isolator Throughput	–0.3
Spatial Mode Mismatch	–0.5
Reflection from AR-coated input and output Fiber Facets (2 @ 98% each)	–0.2
Fiber Attenuation	~0.0
Fiber Polarization Extinction Ratio (15 dB)	–0.1
Bulk Optical Throughput	–1.1
Obscuration (15% Central + 10% Spiders) and Truncation	–1.3
Wavefront Quality (λ/15)	–0.8
Beamwalk	–0.2
Polarization Error (accounted for in Receiver Budget)	NA
Total	-5.6 dB

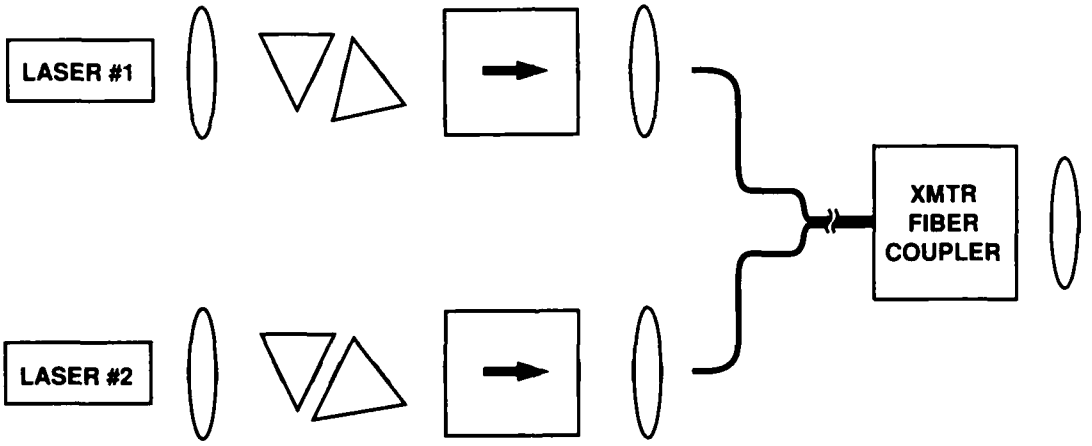

128476-7

Figure 4-5. Fiber-based transmitter.

5. CONCLUSION AND DISCUSSION

The use of fiber optics within space-based lasercom systems offers a number of attractive features over the traditional bulk optics approach. One of the main advantages is the ability to remotely locate the transmitter and receiver from the large front-end optics (i.e., telescope and FSM). This flexibility can lead to reduced size, weight, and stability requirements and allows a modular approach to lasercom system design. For instance, the transmitter module design can proceed somewhat independently of the design of the optical bench.

We have addressed, theoretically and experimentally, a number of key areas of a fiber-based lasercom system. Strawman tracking, receiver, and transmission budgets were presented. Experimental verification of a nutating fiber receiver was presented. Over 1 kHz of closed-loop bandwidth was demonstrated and supplied sufficient rejection to stabilize the line-of-sight disturbances encountered on typical host platforms. The receiver utilized a resonant fiber coupler to perform the nutation function. Theoretical expressions describing communication and tracking performance on nutating depth and relative signal beam diameter were derived. A wide dynamic range transmitter fiber coupler was also constructed and tested. The receiver and transmitter components were then combined in a breadboard duplex fiber-based lasercom system and occupied an area of $< 8 \times 12$ inches. It is expected that with only modest effort this could be reduced by as much as a factor of 2. Acquisition, tracking, pointing, and point-ahead functions were qualitatively demonstrated.

A number of key issues and the collection of more quantitative data remain. For instance, illumination of the uncertainty zone during spatial acquisition and achieving the large (>80 dB) transmitter-to-CCD optical isolation during acquisition need to be addressed. In spite of the outstanding issues, this work indicates that in the next generation of free-space lasercom systems fiber optics may play a strong role.

APPENDIX

In this section we will derive the equations describing the communication and tracking performance as a function of nutation depth and signal beam diameter. It is well known that the mode profile inside a single-mode optical fiber is well approximated as Gaussian. Ignoring the slight ellipticity that is encountered with polarization-preserving fibers, the fiber mode profile (F) after transformation by the focusing lens is represented by

$$F = \sqrt{\frac{2}{\pi\sigma^2}}\, \exp[\, -(\frac{r}{\sigma})^2 - j\,\frac{2\pi}{\lambda} r\,\phi\,(\cos(\theta)\cos(\omega t) + \sin(\theta)\sin(\omega t))\,]$$

$$\sigma = \frac{\lambda\, f}{\pi\, \sigma_f}$$

where σ is the effective 1/e amplitude radius of the fiber mode profile after transformation by the focusing lens, f is the focusing lens focal length, σ_f is the fiber 1/e amplitude radius, r and θ represent the standard polar spatial coordinates, ϕ is the nutation radius, and ω is the nutation frequency, and t is time.

The amplitude distribution of the signal field at the input of the focusing lens for plane wave and Gaussian fields are represented by

$$S = \sqrt{\frac{4\,P_s}{\pi\, d^2}}\, \mathrm{circ}(\frac{2r}{d})\, \exp[\, j\,\frac{2\pi}{\lambda} r\,(\,A\cos(\theta) + E\sin(\theta)\,)\,] \qquad \text{Plane Wave}$$

$$S = \sqrt{\frac{2P_s}{\pi\sigma_s^2}}\, \exp\,[\, -(\frac{r}{\sigma_s})^2 + j\,\frac{2\pi}{\lambda}(\,A\cos(\theta) + E\sin(\theta))\,] \qquad \text{Gaussian}$$

where P_s is the optical signal power, d is the diameter of the signal field for the plane wave case, σ_s is the 1/e amplitude radius of the signal field for the Gaussian case, and A and E are the azimuth and elevation tracking errors.

The coupling profile into the optical fiber is calculated from

$$C(A,E,\phi) = \int_0^{2\pi} d\theta \int_0^{\infty} dr\; r\, F(r,\theta,\phi)\, S(r,\theta)$$

Inserting the expressions for the fiber and signal mode profiles yields

$$C(A,E,\phi) = \sqrt{2P_s}\,\frac{d}{\sigma}\int_0^1 dx\; x\, \exp[-(\frac{dx}{2\sigma})^2]\, J_o[\,\frac{\pi x\,\sqrt{(A-\phi\cos(\omega t))^2 + (E-\phi\sin(\omega t))^2}}{\frac{\lambda}{d}}\,] \qquad \text{Plane Wave}$$

$$C(A,E,\phi) = \sqrt{P_s}\,\frac{2\sigma\sigma_s}{\sigma^2+\sigma_s^2}\exp\left[-\frac{(A-\phi\cos(\omega t))^2 + (E-\phi\sin(\omega t))^2)}{(\frac{\lambda}{\pi})^2(\frac{1}{\sigma^2}+\frac{1}{\sigma_s^2})}\right] \quad \text{Gaussian}$$

Assuming the polarization of the light coupled into the optical fiber is aligned to the LO polarization and that the mode profiles of the signal and LO are the same, an expression describing the normalized signal out of the balanced receiver is given by

$$r = \sqrt{2}\ C(A,E,\phi)\cos(\omega_{if}t) + w(t)$$

$$S_w(f) = \frac{h\nu}{2\eta}$$

where ω_{if} is the heterodyne i.f. frequency, w(t) is the additive white Gaussian shot noise, and $S_w(f)$ is the double-sided spectral density of w(t).

In order to obtain simplified expressions describing communication and tracking performance we will linearize C(A,E, ϕ). In particular, for small tracking errors

$$C(A,E,\phi) \approx C(0,0,\phi) + A\,\frac{\partial C(A,E,\phi)}{\partial A}\Big|_{A=E=0} + E\,\frac{\partial C(A,E,\phi)}{\partial E}\Big|_{A=E=0}$$

Taking advantage of the symmetry between the azimuth and elevation channels the above expression can be rewritten as

$$C(A,E,\phi) \approx m(\phi) + \sqrt{2}\,A\,K(\phi)\cos(\omega t) + \sqrt{2}\,E\,K(\phi)\sin(\omega t)$$

For the plane wave case

$$m(\phi) = \sqrt{2P_s}\,\frac{d}{\sigma}\int_0^1 dx\ x\exp\left[-(\frac{d\,x}{2\sigma})^2\right] J_0(\frac{\pi x\phi}{\frac{\lambda}{d}})$$

$$K(\phi) = \frac{\sqrt{P_s}\,\pi\,\frac{d}{\sigma}\int_0^1 dx\ x^2\exp\left[-(\frac{dx}{2\sigma})^2\right] J_1(\frac{\pi x\phi}{\frac{\lambda}{d}})}{\frac{\lambda}{d}}$$

For the Gaussian case

$$m(\phi) = \sqrt{P_s}\,\frac{2\sigma\sigma_s}{\sigma^2+\sigma_s^2}\exp\left[-\frac{\phi^2}{(\frac{\lambda}{\pi})^2(\frac{1}{\sigma^2}+\frac{1}{\sigma_s^2})}\right]$$

$$K(\phi) = \sqrt{P_s}\,\frac{2\sigma\sigma_s}{\sigma^2+\sigma_s^2}\,\frac{\sqrt{2}\,\phi}{(\frac{\lambda}{\pi})^2(\frac{1}{\sigma^2}+\frac{1}{\sigma_s^2})}\exp[-\frac{\phi^2}{(\frac{\lambda}{\pi})^2(\frac{1}{\sigma^2}+\frac{1}{\sigma_s^2})}]$$

As indicated in Figures 3-1 and 3-3, the output of the balanced receiver, r, is split into two paths; one to the communication system and one to the tracking system. For small tracking errors, the communication performance will be dependent only on $m(\phi)$. The tracking performance is dependent on the particular processing used to derive the angular error estimates. In an ideal nutating tracker receiver, the tracking error estimates would be derived from coherent demodulation of both the heterodyne i.f. frequency (ω_{if}) and the nutation frequency (ω). However, in most coherent lasercom systems this is very difficult due to the low received signal powers. One approach to derive angle error estimates is to incoherently detect the output of the balanced receiver using a square-law detector. If the output of the balanced receiver is approximately given by

$$r = (m(\phi) + K(\phi)A\sqrt{2}\cos(\omega t) + K(\phi)E\sqrt{2}\sin(\omega t))\sqrt{2}\cos(\omega_{if}t) + w(t)$$

If this signal is bandpass filtered around f_{if}, square-law detected, and low-pass filtered to remove the double frequency terms, the resulting signal s is given by

$$s = m(\phi)^2 + 2m(\phi)K(\phi)A\sqrt{2}\cos(\omega t) + 2m(\phi)K(\phi)E\sqrt{2}\sin(\omega t) + n(t)$$

approximately by

$$S_n(f) = 4m(\phi)^2\frac{h\nu}{2\eta} + 4(\frac{h\nu}{2\eta})^2 W$$

and W is the bandwidth of the i.f. filter. To derive an estimate of the azimuth tracking error s is demodulated and normalized to yield

$$[\frac{s\sqrt{2}\cos(\omega t)}{2m(\phi)K(\phi)}]_{LP} \approx A + n'(t)$$

The resulting (single-sided) noise equivalent spectral density of $n'(t)$, which in [8] is referred to as the noise equivalent spectral density (NESD), is given by

$$NESD = \frac{1}{\frac{\eta K(\phi)^2}{h\nu}}\,[\,1 + \frac{1}{2}\frac{W}{\frac{\eta m(\phi)^2}{h\nu}}\,]$$

The noise induced tracking error or noise equivalent angle (NEA) is related to the NESD by [8]

$$NEA = \sqrt{NESD\,NEB}$$

where NEB is the noise equivalent bandwidth of the tracking loop.

REFERENCES

1. E.A. Swanson and R.S. Bondurant, "Fiber-based receiver for free-space coherent optical communications systems," *OFC 1989 Technical Digest*, Optical Fiber Communication Conference, Houston, Texas, February 6-9 (1989).

2. R.J. Feldmann, "Airborne laser communications scintillation measurements and model: A comparison of results," in *Free-Space Laser Communication Technologies*, G.A. Koepf and D.L. Begley (eds.), Proc. SPIE **885,** 24-30 (1988).

3. R.S. Bondurant et al., "An opto-mechanical subsystem for space based coherent optical communication," in *High Data Rate Atmospheric and Space Communication*, T. Hauptman (ed.), Proc. SPIE **996**, 92-100 (1988).

4. M. Wittig, G. Oppenhauser, and A. Hahnen, "Experimental and preoperational optical intersatellite links," in *Free-Space Laser Communication Technologies*, G.A. Koeph and B.L. Begley, (eds.), Proc. SPIE **885**, 42-48 (1988).

5. M. Shikatani et al., "ETS-VI experimental optical inter-satellite communication system," ICC 1989, International Conference on Communications, Boston, MA, June 11-14 (1989).

6. J.H. McElroy et al., "CO_2 laser communication systems for near-earth space applications," IEEE Proc. **65**, 2, 221-251 (1977).

7. J.E. Kaufmann and E.A. Swanson, "Laser intersatellite transmission experiment spatial acquisition, tracking, and pointing subsystem," MIT Lincoln Laboratory, Lexington, Mass., Project Report SC-80, (12 September 1989).

8. E.A. Swanson and J.K. Roberge, "Design considerations and experimental results for direct detection spatial tracking systems," Opt. Eng., **28**, 6, 659-666 (1989).

9. E.A. Swanson et al., "Optical spatial tracking using coherent detection in the pupil-plane," J. of Appl. Opt., **28**, 18, 3918-28 (1989).

10. R. Kern, U. Kugel, and E. Hettlage, "Control of a pointing, acquisition, and tracking subsystem for intersatellite laser links ISL," in *Optical Systems for Space Applications*, H. Lutz and G. Otrio (eds.), Proc. SPIE **810**, 202-210 (1987).

11. C-C Chen and C.S. Gardner, "Impact of random pointing and tracking errors on the design of coherent and incoherent optical intersatellite communication links," IEEE Trans. Commun., **37**, 3, 252-260 (1989).

12. D. Marcuse, "Loss analysis of single-mode fiber splices," Bell Sys. Tech. J., **56**, 6, 703-717 (1976).

13. D. Marcuse, "Gaussian approximation of the fundamental modes of graded-index fibers," J. Opt. Soc. Am., **68**, 1, 103-109 (1984).

14. S. Sarkar, K. Thyagarajan, and A. Kumar, "Gaussian approximation of the fundamental mode in single mode elliptic core fibers," Opt. Commun., **49**, 3, 178-183 (1984).

15. B.J. Klein and J.J. Degnan, "Optical antenna gain. 1: Transmitting antennas," Appl. Opt., **13**, 9, 2134-2141 (1974).

16. B.J. Klein and J.J. Degnan, "Optical antenna gain. 2: Receiving antennas," Appl. Opt., **13**, 10, 2397-2401 (1974).

17. B.J. Klein and J.J. Degnan, "Optical antenna gain. 3: The effect of secondary element support struts on transmitter gain," Appl. Opt., **15**, 4, 977-979 (1976).

18. K.A. Winick and P. Kumar, "Spatial mode matching efficiencies for heterodyned GaAlAs semiconductor lasers," J. Lightwave Technol., **LT-6**, 513 (1988).

19. M. Johnson, "High-precision multiposition single-mode fiber switch using magnetic levitation," SPIE **734** (1987).

20. M. Saruwatari and K. Nawata, "Semiconductor laser to single-mode fiber coupler," Appl. Opt., **19**, 11, 1847-1856 (1979).

21. H.M. Presby et al., "Optical fiber up-tapers with high beam expansion ratios for component fabrication," J. Lightwave Technol., **7**, 5, 820-823 (1989).

22. R.W. Tkach and A.R. Charplyvy, "Regimes of feedback effects in 1.5 μm distributed feedback lasers," J. Lightwave Technol., **LT-4**, 11, 1655-1662 (1986).

23. E. Brinkmeyer, "Analysis of backscattering method for single-mode optical fibers," J. Opt. Soc. Am., **70**, 8, 101-1012 (1980).

24. A.H. Hartog and M.P. Gold, "On the theory of backscattering in single-mode optical fibers," J. Light. Tech., **LT-2**, 2, 76-82 (1984).

25. A.R. Charplyvy, D. Marcuse, and R.W. Tkach, "Effect of Rayleigh backscattering from optical fibers on DFB laser wavelength," J. Lightwave Technol., **LT-4**, 5., 555-559 (1986).

26. H.M. Presby and A. Benner, "Bevelled-microlensed taper connectors for laser and fiber coupling with minimal back-reflections," Electron. Lett., **24**, 18, 1162-1163 (1988).

27. K.L. Hall and R.M. Jopson, "Reducing reflections from single-mode fibers and splices by index-matching or by beveling," AT&T Bell Laboratory.

28. *Optical-Fiber Transmission*, E. E. Basch (ed.), Howard W. Sams & Co., (1986), Chapter 7.

29. G. Smith, "Optical power handling capacity of low loss optical fibers as determined by stimulated Raman and Brillouin scattering," Appl. Opt., **11**, 11, 2489-2494 (1972).

30. D. Cotter, "Stimulated Brillouin scattering in monomode optical fiber," J. Opt. Commun., **4**, 1, 10-19 (1983).

31. Y. Aoki, K. Tajima, and I. Mito, "Input power limits of single-mode optical fibers due to stimulated Brillouin scattering in optical communication systems," J. Lightwave Technol., **6**, 5, 710-719 (1988).

32. R.S. Romaniuk, "Multicore optical fiber components," in *Components for Fiber Optic Applications*, V.J. Tekippe, (ed.), Proc. SPIE **722**, 117-124 (1986).

33. J.A. Taylor et al., "Diode-laser transmitter for space-based heterodyne communication," in *High Data Rate Atmospheric and Space Communications*, R. Hauptman, (ed.), Proc. SPIE, **996**, 77-83 (1988).

34. D. Botez and M. Etterberg, "Beamwidth approximations for the fundamental mode in symmetric double-heterojunction lasers," IEEE J. Quantum Electron., **QE-14**, 11, 827-830 (1978).

35. P. Van Hove and V.W.S. Chan, "Spatial acquisition algorithms and systems for intersatellite optical communication links," MIT Lincoln Laboratory, Lexington, Mass., Technical Report 667, (27 November 1984). DTIC AD-A150794.

36. Katzman, M. (ed.) *Laser Satellite Communication*, Englewood Cliffs, NJ: Prentice-Hall, (1987), Chapter 6.

REPORT DOCUMENTATION PAGE

Form Approved
OMB No. 0704-0188

1. AGENCY USE ONLY *(Leave blank)*	2. REPORT DATE	3. REPORT TYPE AND DATES COVERED
	9 November 1989	

4. TITLE AND SUBTITLE

A Space-Based Optical Communication System Utilizing Fiber Optics

5. FUNDING NUMBERS

F19628-90-C-0002

6. AUTHOR(S)

Eric A. Swanson and Roy S. Bondurant

7. PERFORMING ORGANIZATION NAME(S) AND ADDRESS(ES)

Lincoln Laboratory, MIT
P.O. Box 73
Lexington, MA 02173-9108

8. PERFORMING ORGANIZATION REPORT NUMBER

Technical Report 865

9. SPONSORING/MONITORING AGENCY NAME(S) AND ADDRESS(ES)

Air Force Space Technology Center (AFSTC/SWC)
Kirtland AFB, NM 87117-6006

Electronic Systems Division
Hanscom AFB, MA 01731-5000

10. SPONSORING/MONITORING AGENCY REPORT NUMBER

ESD-TR-89-185

11. SUPPLEMENTARY NOTES

None

12a. DISTRIBUTION/AVAILABILITY STATEMENT

Approved for public release; distribution is unlimited.

12b. DISTRIBUTION CODE

13. ABSTRACT *(Maximum 200 words)*

The use of fiber optics to simplify the design of free-space laser communication systems is explored. The potential advantages of fiber optics within free-space optical communication systems are not widely recognized. The current generation of spaceborne optical communication systems relies on the use of bulk optics rigidly mounted to an optical bench to get light from the optical sources to the exit aperture or from the entrance aperture to the optical receiver. These designs are all very sensitive to thermal and mechanical perturbations as well as to the detailed dynamic characteristics of the host spacecraft. Optical fibers can provide the means to remotely locate the transmitter lasers, local oscillator (LO) lasers (in the case of a coherent system), and the receiver from the front-end optics. This allows flexibility in the mechanical design which can reduce the size, weight, and stability requirements of the overall system.

This paper presents an overview of a fiber-based free-space lasercom system and contrasts this proposed technology to the present technology. Detailed design considerations concerning the issues of pointing, tracking, and receiver communication performance are presented. Other key areas such as efficient source-to-fiber coupling, isolation, transmitter power limitations, and acquisition are highlighted. Preliminary experimental results of our breadboard fiber-based coherent optical communication system are also presented.

14. SUBJECT TERMS		15. NUMBER OF PAGES
spatial tracking	fiber optics	52
optical communication	precision pointing	16. PRICE CODE
intersatellite optical links		

17. SECURITY CLASSIFICATION OF REPORT	18. SECURITY CLASSIFICATION OF THIS PAGE	19. SECURITY CLASSIFICATION OF ABSTRACT	20. LIMITATION OF ABSTRACT
Unclassified	Unclassified	Unclassified	